J. Fluid Mech. (1997), *vol.* 338, *pp.* 317–340. Printed in the United Kingdom

© 1997 Cambridge University Press

Erosion by planar turbulent wall jets

By ANDREW J. HOGG, HERBERT E. HUPPERT AND W. BRIAN DADE

Institute of Theoretical Geophysics, Department of Applied Mathematics and Theoretical Physics, University of Cambridge, Silver Street, Cambridge CB3 9EW, UK

(Received 28 June 1996 and in revised form 13 December 1996)

New scaling laws are presented for the spatial variation of the mean velocity and lateral extent of a two-dimensional turbulent wall jet, flowing over a fixed rough boundary. These scalings are analogous to those derived by Wygnanski *et al.* (1992) for the flow of a wall jet over a smooth boundary. They reveal that the characteristics of the jet depend weakly upon the roughness length associated with the boundary, as confirmed by experimental studies (Rajaratnam 1967).

These laws are used in the development of an analytical framework to model the progressive erosion of an initially flat bed of grains by a turbulent jet. The grains are eroded if the shear stress, exerted on the grains at the surface of the bed, exceeds a critical value which is a function of the physical characteristics of the grains. After the wall jet has been flowing for a sufficiently long period, the boundary attains a steady state, in which the mobilizing forces associated with the jet are insufficient to further erode the boundary. The steady-state profile is calculated separately by applying critical conditions along the bed surface for the incipient motion of particles. These conditions invoke a relationship between the mobilizing force exerted by the jet, the weight of the particles and the local gradient of the bed. Use of the new scaling laws for the downstream variation of the boundary shear stress then permits the calculation of the shape of the steady-state scour pit. The predicted profiles are in good agreement with the experimental studies on the erosive action of submerged water and air jets on beds of sand and polystryene particles (Rajaratnam 1981).

The shape of the eroded boundary at intermediate times, before the steady state is attained, is elucidated by the application of a sediment-volume conservation equation. This relationship balances the rate of change of the bed elevation with the divergence of the flux of particles in motion. The flux of particles in motion is given by a semi-empirical function of the amount by which the boundary shear stress exceeds that required for incipient motion. Hence the conservation equation may be integrated to reveal the transient profiles of the eroded bed. There is good agreement between these calculated profiles and experimental observations (Rajaratnam 1981).

1. Introduction

When jets impinge upon loose beds of granular material, they can lead to significant local scour. For example, the plunging water flow found under dam spillways leads to the erosion of the channel bed and to the possible weakening of engineered structures (Mason & Arumugam 1985). However jet-induced scour is not always undesirable; recently developed dredging vessels use high-velocity water jets to mobilize accumulated sediment. The jets entrain the sedimentary particles from the bed to form a

https://doi.org/10.1017/S0022112097005077 Published online by Cambridge University Press

cloud of a higher density than the surrounding fluid. This density difference initiates a flow which transports the sediment away from the region being dredged.

There are many physical processes that are pertinent to the erosion of a loose bed of grains by jet impingement. These include the vigour of the jet-induced fluid turbulence, the pressure and shear stress distribution exerted on the bed, the density and size of the particles and the angle of repose of the granular material comprising the bed. The coupling between the shape of the eroded pit and the characteristics of the jet flow render this problem highly complex. Most of the previous studies have been experimental and have attempted to model the erosion theoretically in an empirical manner. Several studies have been conducted by Rajaratnam and co-workers (Rajaratnam & Berry 1977; Rajaratnam & Beltaos 1977; Rajaratnam 1981, 1982; Rajaratnam, Aberibigbe & Pochylko 1995) in papers which discuss laboratory observations of scour pits arising from jet impingement. The experiments were carried out using submerged water and air jets, which impinged on beds composed of particles of sand and polystryene. Other studies have focused on particular issues of this erosion process. Kobus, Leister & Westrich (1979) studied pulsating jets and demonstrated that these can lead to greater erosion than steady jets. Mih & Kabir (1983) studied the erosion of beds of mixed particle size; they were interested in the problem of removing sand grains from between larger pebbles which form the breeding ground for salmon. Stein, Julien & Alonso (1993) modelled the time-dependent problem to track the evolution of the maximum eroded scour depth.

In this study we focus on the erosion of a loose bed of non-cohesive granular material by a two-dimensional turbulent wall jet. We assume that the axis of the jet is parallel to the initial surface of the bed and that the source of the jet momentum is close to the bed. This leads to a considerable simplification of the problem because it allows us to assume that the forces which mobilize the particles from the boundary are just those associated with the shear stress. A model of the progressive erosion of an initially flat bed of grains was developed and we find that the eroded profile attains an equilibrium shape that can be computed separately from the time-dependent calculation. The dimensions of this steady-state profile are related in a simple way to the hydrodynamic properties of the jet and the size, excess density and angle of repose of the particles. This analysis permits the steady-state profiles of both water and air jets to be modelled using the same framework, although the particles may be transported out of the scour pit in different ways (Rajaratnam 1981).

In the next section we consider the flow of turbulent wall jets over fixed boundaries. To this end, the analysis of Wygnanski, Katz & Horev (1992) for flows of turbulent wall jets over smooth boundaries are reviewed. We then develop new scaling laws to predict the spatial variation of the jet characteristics for flows of turbulent jets over boundaries of a given grain roughness; these new scalings are analogous to those proposed by Wygnanski *et al.* (1992). We find that these account for the weak dependence on roughness length found in the experiments of Rajaratnam (1967). In §3 we derive critical conditions for the incipient motion of loose particles in repose on a bed with a longitudinal slope. This establishes a relationship between the mobilizing force associated with the jet flow, the weight of the particles and the local gradient of the bed. We apply the jet flow scaling over fixed rough boundaries to erodible boundaries, on the assumption that the aspect ratio of the pit is small. (Here the aspect ratio is defined as the ratio of depth to streamwise extent). In this way we calculate the dimensions of the steady-state pit (§4). In §5 we utilize a semi-empirical model for the flux of transported particles to study the temporal evolution of the scour starting from an initially horizontal boundary. This calculation elucidates the

https://doi.org/10.1017/S0022112097005077 Published online by Cambridge University Press

rate of evolution of the maximum eroded depth. Finally, in §6, we summarize our findings.

2. The flow of two-dimensional turbulent wall jets

2.1. *Smooth fixed boundaries*

We consider the flow of a steady two-dimensional turbulent jet along a horizontal boundary. This kind of 'wall jet' flow may be treated as a boundary layer flow to which momentum has been added upstream of the region of interest. This view implies that the velocity over some range in the shear layer exceeds that in the free stream (Launder & Rodi 1983). The flow has been modelled by the boundary-layer equations (Rajaratnam 1976), on the assumption that the pressure is constant with distance normal from the boundary and the streamwise variations of normal stress are negligible. In this case we further assume that the flow is driven by the upstream source of momentum, rather than any streamwise pressure gradient. Therefore denoting the horizontal and vertical coordinates by x and y, the mean horizontal and vertical velocities by u and v, the fluid density by ρ and the mean shear stress by τ, the Reynolds-averaged equations describing the flow are the streamwise conservation of momentum and the continuity equation, given by

$$u\frac{\partial u}{\partial x}+v\frac{\partial u}{\partial y}=\frac{1}{\rho}\frac{\partial \tau}{\partial y} \tag{2.1}$$

and

$$\frac{\partial u}{\partial x}+\frac{\partial v}{\partial y}=0. \tag{2.2}$$

The boundary conditions specify the upstream streamwise momentum flux, ρM_0, the no-slip condition on the boundary and the decay of the streamwise velocity away from the boundary, which may be expressed as

$$\int_0^\infty \rho u^2\,\mathrm{d}y=\rho M_0 \qquad (x=0), \tag{2.3}$$

$$u=v=0 \qquad (y=0) \tag{2.4a,b}$$

and

$$u\to 0 \quad (y\to\infty). \tag{2.5}$$

For purely viscous stresses, there exists a similarity solution for the velocity fields (Glauert 1956). For turbulent wall-jet flows, there is no consensus on the appropriate closure for the turbulent stresses and so the velocity distribution cannot be predicted with any certainty. There are, however, a number of proposed empirical distributions (Launder & Rodi 1983). This uncertainty illustrates the important distinction between the wall-jet flow and a fully developed turbulent boundary layer. In the latter, the shear stress is approximately constant in a region close to the boundary and the horizontal velocity varies logarithmically with height. In a wall jet, however, there is no equivalent constant-stress layer.

The lack of an analytical framework for the prediction of the variation of the velocity field implies that the boundary shear stress, τ_b, cannot be predicted accurately. However, by integrating the momentum equation (2.1), it is found that

$$\tau_b=-\frac{\mathrm{d}}{\mathrm{d}x}\int_0^\infty \rho u^2\,\mathrm{d}y. \tag{2.6}$$

https://doi.org/10.1017/S0022112097005077 Published online by Cambridge University Press

There have been a number of papers which consider the variation of the maximum horizontal velocity, u_m, and the height above the boundary, δ, at which this velocity is attained (Launder & Rodi 1983). Traditionally it has been assumed that $u_m \sim (M_0/x)^{1/2}$ and $\delta \sim x$. These are the scalings of a two-dimensional free jet, sufficiently far downstream of the jet source. They arise from the hypotheses that molecular viscosity does not play a role in the evolution of the jet (i.e. the Reynolds number based on nozzle width is large) and the streamwise momentum flux is constant. Neither of these assumptions is valid for a wall jet. The boundary shear stress, given by the streamwise rate of change of the momentum flux (2.6), is non-negligible. Hence the momentum flux is not constant. Furthermore, the presence of the boundary introduces a no-slip condition on the flow (equation (2.4)). Therefore, in accord with Wygnanski *et al.* (1992), we conclude that the two-dimensional parameters governing the evolution of the flow are the initial streamwise momentum flux per unit mass $M_0 \equiv b_0 U_0^2$ and the kinematic viscosity ν. (Here we have equated the initial momentum flux with the product of the nozzle width, b_0, and the square of the initial velocity, U_0.) The evolution of the velocity and boundary-layer thickness of the flow are then given by

$$u_m = F_1(M_0, \nu, x) \qquad \text{and} \qquad \delta = F_2(M_0, \nu, x), \tag{2.7a, b}$$

where F_1 and F_2 are arbitrary functions. Writing these in dimensionless variables and assuming the functions take a power-law form, Wygnanski *et al.* (1992) proposed that

$$u_m = C_1 M_0/\nu (M_0 x/\nu^2)^{-m} \qquad \text{and} \qquad \delta = C_2 \nu^2/M_0 (M_0 x/\nu^2)^n, \tag{2.8a, b}$$

where C_1 and C_2 are constants. Hence, in terms of the Reynolds number based on jet-nozzle width, $Re = U_0 b_0/\nu$,

$$u_m/U_0 = C_1 (b_0/x)^m Re^{1-2m} \qquad \text{and} \qquad \delta/b_0 = C_2 (x/b_0)^n Re^{2(n-1)}. \tag{2.9a, b}$$

Wygnanski *et al.* (1992) found that without adjusting for virtual origin effects to account for the establishment of the flow, the exponents in these relationships are given by $m = 0.47$ and $n = 0.88$. Hence the effect of viscous forces is to reduce the rate of decay of the jet velocity. Presumably the exponents m and n are functions of the Reynolds number so that as $Re \to \infty$, $m \to \frac{1}{2}$, $n \to 1$ and the scaling recovers that of the free jet. Wygnanski *et al.* (1992) also found that by use of (2.6), the boundary shear stress varies as

$$\tau_b \sim \rho (M_0/\nu)^2 (M_0 x/\nu^2)^{2(-0.47)+0.88-1}.$$

Rajaratnam (1976) and Wygnanski *et al.* (1992) demonstrate that if a dependence of the velocity upon downstream distance, similar to that of a free jet (i.e. $m = 1$), had been sought, then the residual constant of proportionality C_1 is weakly dependent upon Reynolds number. However by use of the new scaling (2.9), this Reynolds number dependence of C_1 is eliminated.

2.2. *Rough fixed boundaries*

This new scaling for the behaviour of wall jets is now applied to those for which the flow is over a boundary of a prescribed roughness. If a boundary is artificially roughened by particles of a given diameter, then the bed roughness, k_e, which is the lengthscale of protrusions into the flow, is simply proportional to the particle diameter. Furthermore, if these protrusions extend to far outside the laminar sublayer, then most of the resistance to the flow arises from the form drag associated with the individual elements, rather than the viscous drag. In this case the flow is termed

https://doi.org/10.1017/S0022112097005077 Published online by Cambridge University Press

as 'hydraulically rough' (Fredsøe & Deigaard 1992). Rajaratnam (1967) performed experiments on such wall jets and in this subsection we analyse his results. First, we suppose that the normalized maximum mean velocity, u_m/U_0, and boundary-layer thickness, δ/b_0, are only dependent upon the downstream position x/b_0 as plotted in figure 1. We find that there is considerable scatter in the data, which remains even after the data for which $x/b_0 < 5$ are excluded. These exclusions are justified because within a downstream distance from the jet source of the order of only a few (~ 5) nozzle widths the flow has not fully developed; the turbulence arising from the mixing of the jet and the ambient fluid has not penetrated throughout the entire width of the jet. This region of flow development is referred to as the potential core. Rajaratnam (1976) suggests that the potential core extends downstream to a distance of approximately 6 nozzle widths. Hence these data are excluded.

We hypothesise that the dimensional variables which govern the flow are the initial streamwise momentum flux per unit mass M_0 and a measure of the turbulent viscosity associated with the roughness elements given by $U_0 k_e$, where k_e is the roughness length and is proportional to grain size. For flows over rough boundaries it is not the fluid viscosity which ultimately influences the flow because the roughness elements prevent the establishment of a viscous boundary layer. Rather the turbulent viscosity based on roughness length is the relevant parameter to indicate how the no-slip boundary condition is enforced. Strictly this eddy viscosity is given by $u_* k_e$ where u_* is the friction velocity. However, there is no initial measure of u_* and so we use U_0 instead. In non-dimensional and power-law form we seek the following relationships:

$$u_m = C_3 M_0/U_0 k_e (x M_0/U_0^2 k_e^2)^{-m} \qquad \text{and} \qquad \delta = C_4 U_0^2 k_e^2/M_0 (x M_0/U_0^2 k_e^2)^n, \quad (2.10a,b)$$

where C_3 and C_4 are constants. Hence we find that

$$u_m/U_0 = C_3 (x/b_0)^{-m} (b_0/k_e)^{1-2m} \qquad \text{and} \qquad \delta/b_0 = C_4 (x/b_0)^n (b_0/k_e)^{2(n-1)}. \quad (2.11a,b)$$

From the plots of Rajaratnam's data presented in figure 2, we find the exponents are $m = 0.47$ and $n = 0.84$. Hence the variation of the maximum velocity and the boundary-layer thickness of the flow are only weakly dependent on the roughness because the exponents differ only slightly from the free-jet case of $m = 0.5, n = 1$. We note that the collapse of these plots is improved by removing those points which fall within the flow development region ($x/b_0 < 5$). We note the remarkable correspondence between the numerical value of the exponents for the rough and smooth boundaries. By use of equation (2.6), we find that the boundary shear stress is given by

$$\tau_b = C_5 \rho U_0^2 (x/b_0)^{-2m+n-1} (b_0/k_e)^{2(n-2m)}, \quad (2.12)$$

where C_5 is a constant. Since the roughness is related to the size of the particles which comprise the roughened boundary, we find that the size of the particles influences both the growth of the boundary layer and the decay of the maximum velocity. This is inevitable: given that viscosity plays a role in the flows over the hydraulically smooth boundaries, then for rough boundaries the particle size must also play a role because it influences the vertical diffusion of the horizontal momentum within the flow.

3. Conditions for incipient motion

We identify critical conditions for incipient particle motion by calculating the moments of the forces which drive and resist particle motion. The forces leading to particle motion on the surface of the bed of grains arise from the shear stress

https://doi.org/10.1017/S0022112097005077 Published online by Cambridge University Press

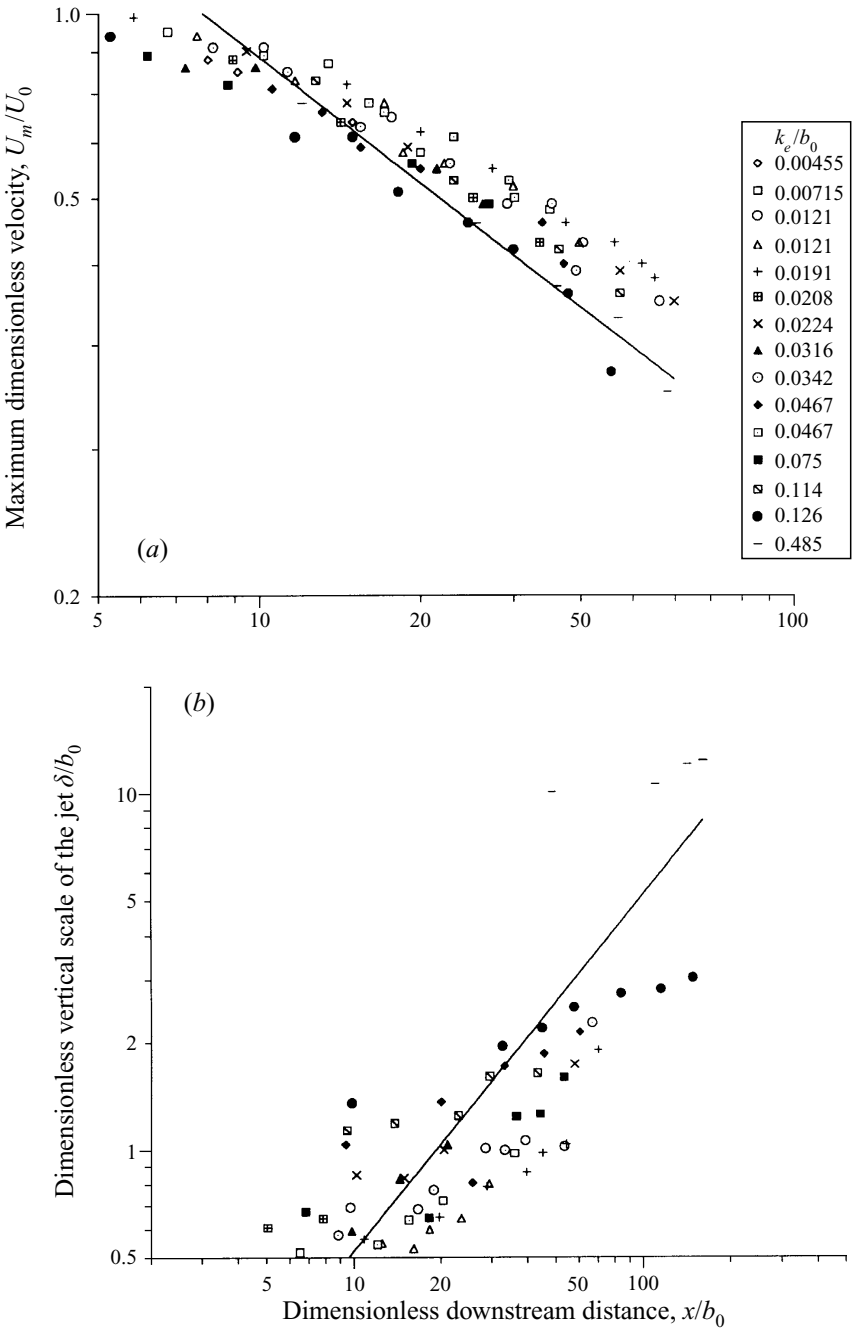


FIGURE 1. (*a*) The variation of the maximum wall-jet velocity and (*b*) the boundary-layer thickness of the wall jet as functions of the downstream distance from the source and the roughness of the boundary (k_e). (The boundary-layer thickness is the distance from the boundary at which the average downstream velocity attains its maximum value.) The downstream distances and boundary-layer thicknesses are non-dimensionalized with respect to the the nozzle width, b_0, and the maximum velocities are non-dimensionalized with respect to U_0, where the horizontal momentum flux per unit mass is given by $M_0 = b_0 U_0^2$. The curves are the best-fit lines of the form $U_m \sim (M_0/x)^{1/2}$ and $\delta \sim x$. The equations of the curves are (*a*) $U_m/U_0 = 2.8(b_0/x)^{1/2}$ and (*b*) $\delta/b_0 = 0.05x/b_0$. (Data from Rajaratnam 1967.)

https://doi.org/10.1017/S0022112097005077 Published online by Cambridge University Press

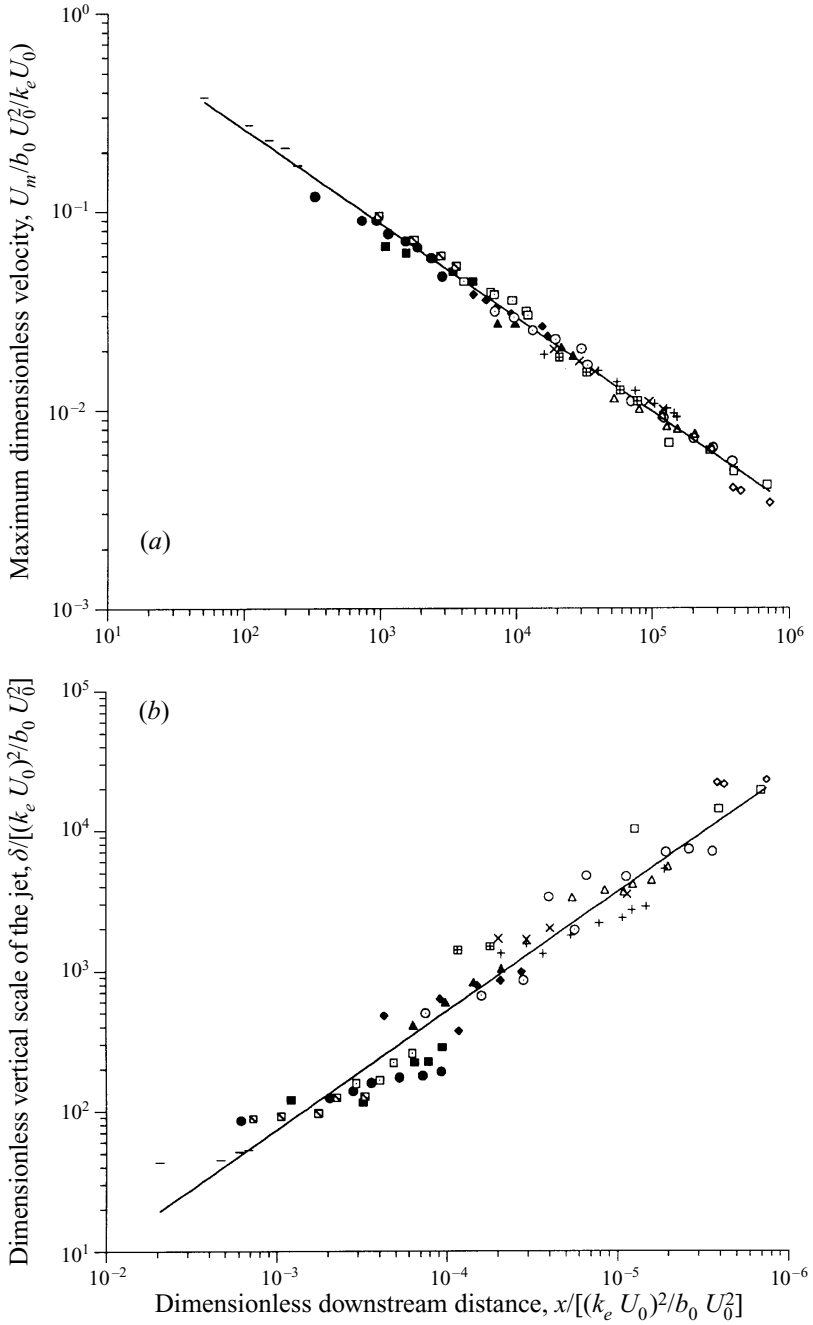


FIGURE 2. (*a*) The variation of the maximum wall-jet velocity and (*b*) the boundary-layer thickness of the wall jet as functions of the downstream distance from the source and the roughness of the boundary (k_e). Data points for which $x/b_0 < 5$ are omitted. The downstream distances are non-dimensionalized with respect to k_e^2/b_0 and the maximum velocities are non-dimensionalized with respect to b_0U_0/k_e (see §2 for an explanation of these scales). The curves are the best-fit curves of the form $U_m/(b_0U_0/k_e) \sim [x/(k_e^2/b_0)]^m$ and $\delta/(k_e^2/b_0) \sim [x/(k_e^2/b_0)]^n$. The equations of the curves are (*a*) $U_m/(b_0U_0/k_e) = 2.3[x/(k_e^2/b_0)]^{-0.475\pm0.005}$ and (*b*) $\delta/(k_e^2/b_0) = 0.21[x/(k_e^2/b_0)]^{0.84\pm0.025}$. The confidence limits on the exponents are given by the standard errors of the best-fit values. (Data from Rajaratnam 1967). Symbols as in figure 1.

https://doi.org/10.1017/S0022112097005077 Published online by Cambridge University Press

exerted by the jet flow, whereas the particle weight resists motion. This implies that the jet flow introduces negligible flow within the porous granular bed. Luque (1974) and Wiegel (1980) argue that the effects within the bed of a shear flow parallel with the bed surface are rapidly attenuated. This is not the case, however, if the jet flow impinges upon the bed. Such an impingement leads to a surface pressure distribution and a seepage flow within the bed (Kobus *et al.* 1979). In this case the mobilizing force is a more complex function of the surface pressure, bed shear stress and bed permeability.

Consider the idealized scenario of a bed composed of identical spherical particles, as depicted in figure 3. The angle of inclination of the bed is denoted by β and the horizontal and vertical forces driving particle motion by $F_x = C_D \pi d^2 \tau_b \cos\beta$ and $F_y = C_D \pi d^2 \tau_b \sin\beta$, where C_D is a constant drag coefficient. The submerged weight of a particle is given by $W = \frac{1}{6}\pi d^3 \Delta\rho g$, where $\Delta\rho$ is the excess density of the particle. (We have ignored the possibility of a lift force on the particles; this could be simply included by the introduction of a suitable lift coefficient.) We consider the moment of these forces exerted on a single particle in repose on the bed surface about its point of contact with a neighbouring particle. The moment of inertia of a particle about the axis passing through this point of contact is denoted by I, the angular velocity of the particle by ω and the angle of repose of the granular material by α. Readers will find further details of this calculation in the Appendix. We find there that

$$I\frac{\mathrm{d}\omega}{\mathrm{d}t} = \tfrac{1}{2}d\left(F_x\cos(\alpha+\beta) + F_y\sin(\alpha+\beta) - W\sin(\alpha+\beta)\right). \tag{3.1}$$

For particle motion, we require that $\mathrm{d}\omega/\mathrm{d}t > 0$ and hence that

$$\tau_b C_D \cos\alpha > \tfrac{1}{6}\Delta\rho g d \sin(\alpha+\beta). \tag{3.2}$$

This expression for the incipient motion of particles on a bed with a longitudinal slope links the shear stress exerted by the jet with the local gradient of the bed and excess density, size and angle of repose of the particles. We note that if the downward inclination of the bed exceeds the angle of repose ($-\beta > \alpha$), then the particles are inevitably in motion. An equivalent expression was derived by Luque (1974) and by Kovacs & Parker (1994) for a particle on a surface with both lateral and longitudinal gradients. We present an alternative derivation of the critical conditions for particle motion on a bed with a generalized slope in the Appendix. This yields the same final expressions as Kovacs & Parker (1994), but is derived in terms of turning moments and the angle of repose, rather than forces and the coefficient of friction.

Shields (1936) examined conditions for the incipient motion of particles from a flat bed ($\beta = 0$). He found the critical value of the ratio $\theta_{crit} = \tau_b/\Delta\rho g d$ for incipient motion. In terms of the analysis above, this critical ratio is given by $\theta_{crit} = \frac{1}{6}\tan\alpha/C_D$. Shields found that this critical value attains an approximately constant value when the particle Reynolds number is sufficiently large and that its value is different for experiments performed in air and water. For water, $\theta_{crit} \approx 0.05$ (Nielsen 1992), whereas for air, $\theta_{crit} \approx 0.025$ (Greeley & Iversen 1985). Denoting the critical value of the ratio $\tau_b/\Delta\rho g d$ for incipient motion on a bed with a longitudinal gradient by θ_c, we find that

$$\theta_c = \theta_{crit}\frac{\sin(\alpha+\beta)}{\sin\alpha}. \tag{3.3}$$

The boundary shear stresses are turbulent and although attaining a steady mean value, the instantaneous stresses are highly intermittent. These fluctuations are analogous to the turbulent events found within boundary layers (Kline *et al.* 1967).

https://doi.org/10.1017/S0022112097005077 Published online by Cambridge University Press

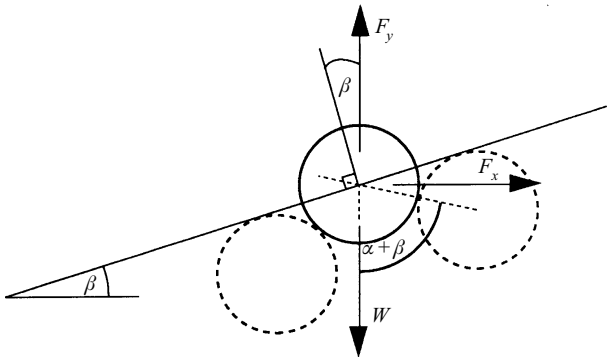


FIGURE 3. The forces acting on a particle in repose on the surface of a bed at an angle β to the horizontal. (The angle of repose of the granular medium is denoted by α.)

Hence it is possible that the 'steady' profile of the eroded boundary will be only a dynamic equilibrium. The shear stress, at times, may significantly exceed its mean, leading to additional particle movement. This may in turn lead to the eroded profile adopting local positive gradients which exceed the angle of repose (i.e. $\beta > \alpha$). However, between the times when the stress attains a value in excess of the mean, it drops to a much lower value and cannot support the high gradient of the eroded bed. Hence the bed relaxes back to the angle of repose (i.e. $\beta = \alpha$).

Rajaratnam (1981) performed erosion experiments using both air and water wall jets. In order to assess in which of these two media this relaxation process is going to be of greater importance, we consider the timescale of angular acceleration of the particle. This may be estimated from (3.1) and is given by

$$S = \frac{\rho_s}{\Delta\rho}\left(\frac{d}{g}\right)^{1/2}. \tag{3.4}$$

Hence, the ratio of these two timescales in air and water for particles of a similar size and density is given by

$$S_{air}/S_{water} = \frac{\rho_s - \rho_{water}}{\rho_s - \rho_{air}} < 1. \tag{3.5}$$

This implies that the grains in air exhibit a more rapid angular acceleration than those in water due to an applied moment with the same value of the ratio $\tau_b/\Delta\rho g d$. Thus for the experiments performed with jets of air, we expect that the gradients of the eroded scour pits are more likely to undergo this relaxation process than those with water jets. This implies that the upward gradients are more likely to have an upper bound (i.e. the angle of repose), because they rapidly adjust during the times when the shear stress falls below its mean value. This rationalizes the observation of Rajaratnam (1981) that the steady-state eroded profiles for experiments with the wall jets of water were significantly different when the jet was flowing than when it was stopped. Conversely, for the experiments with the jets of air, there was little difference. While both water and air jets generate instantaneous shear stresses which can support eroded profiles with upward gradients in excess of the angle of repose ($\beta > \alpha$), those generated using jets of air have a greater tendency to relax to the angle of repose during the intermittent periods of low shear stress. When the jet is stopped, the profiles adjust to a state in which all the gradients are limited by the angle of repose. This adjustment, therefore, will appear more significant for the experiments

https://doi.org/10.1017/S0022112097005077 Published online by Cambridge University Press

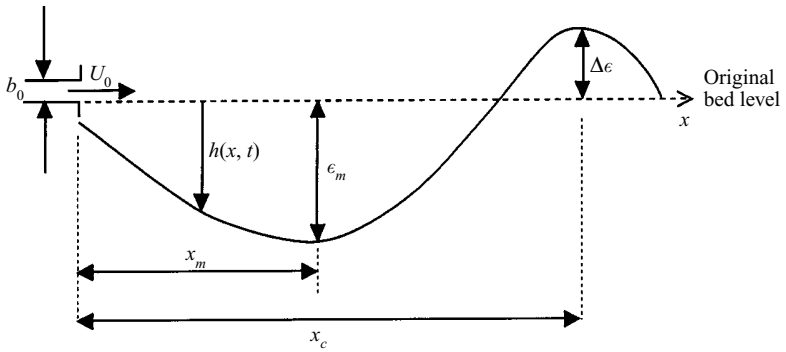


FIGURE 4. Sketch of the wall jet and the resulting scour pit with its important dimensions.

with water jets. This process also explains why Rajaratnam (1981) found a reduction of the maximum depth eroded by a water jet when the jet was stopped.

4. Steady-state profiles

Armed with the concept of a mobilization criterion on a bed with a longitudinal slope (§3), we investigate the erosion of a granular bed by a two-dimensional turbulent jet. The bed is initially planar and the jet flows in a direction that is parallel to this surface, through what is otherwise quiescent ambient fluid. The jet flow erodes the bed and, in this section, we investigate the shape of the erosion profiles which are invariant with time: the steady-state profiles. We begin by predicting the dimensions of these scour pits, as depicted in figure 4, in terms of the characteristics of the jet and the particles.

The profile of the scour pit can be calculated by considering the shear stress distribution along the surface of the bed. We further assume that the boundary shear stress for the flow of a two-dimensional jet over an erodible boundary is equivalent to the flow of a two-dimensional jet over a fixed rough boundary, as given by (2.12). In making this crude approximation, we assume that the boundary profile has negligible influence on the jet flow; or equivalently, that the aspect ratio of the eroded profile is small. In fact, any bed topography will exert an additional drag on the flow, leading to a more rapid attenuation of the boundary shear stress. Furthermore, we assume that the mean flow does not separate from the boundary at any downstream location to avoid the need to introduce models of regions in which the flow recirculates. This assumption is inappropriate for flow over the crest of the eroded profile (i.e $x > x_c$). Recognizing that these assumptions constitute considerable simplifications, we postulate that the shear stress is given by

$$\tau_b = C_6 \rho U_0^2 (b_0/d)^{2\gamma} (x/b_0)^{-1+\gamma} G(h, x), \tag{4.1}$$

where C_6 is a constant which is different from C_5 in equation (2.12) due to the replacement of the surface roughness with the diameter of the particles. Also $y = h(x)$ is the profile of the boundary, $\gamma = n - 2m$ and $G(h, x)$ is a shape function to encapsulate how the boundary shear stress varies when the boundary is no longer horizontal. Initially the boundary is flat ($h = 0$) and so we require that $G(0, x) = 1$, but other than this there is no available model or data to prescribe the variation of

https://doi.org/10.1017/S0022112097005077 Published online by Cambridge University Press

G. We therefore propose the following Gaussian-like model of the stress distribution:

$$G(h,x) = \begin{cases} 1 & (h \geqslant 0), \\ \exp\left(-(h/C_7\delta)^2\right) & (h < 0), \end{cases} \tag{4.2a,b}$$

where C_7 is a constant and $\delta(x)$ is the boundary-layer thickness, which varies with downstream position. We have set $G(h,x) = 1$ for $h \geqslant 0$ since the wall jet is simply deflected upwards without altering the magnitude of the shear stress, whereas for $h < 0$ we assume that the shear stress varies with Gaussian-like characteristics. We emphasize that this is a somewhat arbitrary model of the shear stress distribution and that within this analytical framework any other shape function could be used. Indeed our preliminary investigations indicate that there is little difference in the results introduced by the use of an alternative model .

Critical conditions for motion on a sloping bed are given by

$$\Theta(x/b_0)^{-1+\gamma} G(h,x) \geqslant \frac{\sin(\alpha+\beta)}{\cos\alpha}, \tag{4.3}$$

where Θ is an erosion parameter defined by $\Theta = C_6\rho U_0^2 (b_0/d)^{2\gamma} \tan\alpha/\Delta\rho g d\theta_{crit}$. Hence for the equilibrium profile attained by the eroding wall jet, we impose the equality of (4.3) along the boundary $y = h(x)$, with the local gradient of the bed given by $\mathrm{d}h/\mathrm{d}x = \tan\beta$.

At this stage of the analysis it is convenient to non-dimensionalize the lengthscales and the shear stresses by writing

$$\xi = (x/b_0)\Theta^{-1/(1-\gamma)}, \tag{4.4}$$

$$\eta = (h/b_0)\Theta^{-1/(1-\gamma)}, \tag{4.5}$$

$$f_b = \tau_b \tan\alpha/\Delta\rho g d\theta_{crit}, \tag{4.6a}$$

$$= \xi^{-1+\gamma} \begin{cases} 1 & (\eta \geqslant 0), \\ \exp\left(-\eta^2/\sigma^2\xi^{2n}\right) & (\eta < 0), \end{cases} \tag{4.6b,c}$$

where $\sigma = C_7 C_4 \Theta^{(n-1)/(1-\gamma)} (b_0/d)^{n-1}$. Hence the profile of the boundary is given by

$$f_b = \frac{\mathrm{d}\eta/\mathrm{d}\xi + \tan\alpha}{[1 + (\mathrm{d}\eta/\mathrm{d}\xi)^2)]^{1/2}}, \tag{4.7}$$

which may be re-written as

$$\frac{\mathrm{d}\eta}{\mathrm{d}\xi} \equiv \tan\beta = \frac{-\tan\alpha + [\tan^2\alpha - (f_b^2 - 1)(f_b^2 - \tan^2\alpha)]^{1/2}}{f_b^2 - 1}, \tag{4.8}$$

subject to boundary conditions which represent the absence of erosion far from the jet source (4.9) and the conservation of the volume of particles (4.10),

$$\eta(\xi^*) = 0 \tag{4.9}$$

and

$$\int_0^{\xi^*} \eta \, \mathrm{d}\xi = 0. \tag{4.10}$$

There are two remaining non-dimensional parameters in this system of equations for the rescaled dimensions of the scour pit, namely σ and $\tan\alpha$. The magnitude of the first of these indicates the rate of expansion of the wall jet as it flows downstream. It is a function of the rate at which ambient fluid is entrained into the jet.

https://doi.org/10.1017/S0022112097005077 Published online by Cambridge University Press

4.1. *Extent of eroded zone* ($\xi = \xi_c$)

We identify the extent of the eroded zone as where the boundary has attained its peak value and is locally flat ($\beta = 0$). Hence we find that

$$\xi_c^{-1+\gamma} = \tan\alpha. \tag{4.11}$$

Therefore, in terms of the dimensional variables

$$\frac{x_c b_0}{d^2} = \theta_{crit}^{-1/(1-\gamma)} \left(\frac{C_6 \rho U_0^2 b_0^2}{\Delta \rho g d^3} \right)^{1/(1-\gamma)}. \tag{4.12}$$

We plot on figure 5*a* the data for the air and water experiments on a log-log graph of $x_c b_0/d^2$ against $\Upsilon \equiv \rho U_0^2 b_0^2/\Delta\rho g d^3$. We note that the curves for the two media have similar exponents, as predicted by (4.12), and differ by a constant factor of approximately 2. Furthermore, if we assume that the shear stress varies with distance from the nozzle in a similar way to the wall-jet flows over horizontal rough boundaries, then $1/(1-\gamma) = 0.90$, which compares favourably with the measured value of 0.85. Also the constant factor may be rationalized in terms of the different critical Shields parameters θ_{crit} for the incipient motion for the two media. The ratio $(\theta_{crit\ water}/\theta_{crit\ air})^{1/(1-\gamma)} \approx 2$ and this is approximately equal to the ratio of the empirically fitted constants (see figure 5*a*).

These results are to be contrasted with the analysis of Rajaratnam (1981) in which he suggests a linear correlation between x_0/b_0 and $F_0 = U_0/(\Delta\rho g d/\rho)^{1/2}$. Not only do we find that the correlation given by (4.12) yields an improved collapse of the data, but also that the differences between the data for water and for air may be rationalized in terms of the critical Shields parameter pertaining to the different media.

4.2. *Downstream distance to the position of maximum eroded depth* ($\xi = \xi_m, \eta = \eta_m$)

The downstream location of the maximum eroded depth may be calculated from (4.8) by seeking the minimum of the function $\eta(\xi)$. This leads to the requirement that at the maximum eroded depth

$$\xi_m^{-1+\gamma} \exp\left(-\frac{\eta_m^2}{\sigma^2 \xi_m^{2n}} \right) = \tan\alpha. \tag{4.13}$$

In this expression ξ_m is an implicit function of n and σ, where σ is itself a weak function of Θ and b_0/d. We henceforth simplify this equation by setting the exponent n equal to unity. This fixes the empirical shape function G for the stress distribution and renders the parameter σ independent of the flow and particle characteristics. This simplification has only negligible influence on the interpretation of the experimental results of Rajaratnam (1981), because the dependence on the exponent n occurs in only the shape function. Furthermore, as found in §2, we expect $|1-n| \ll 1$ and the experiments performed with an erodible boundary do not provide sufficient resolution to permit an accurate assessment of the value of n.

On the assumption that $\eta_m/\sigma\xi_m$ is approximately constant, which is demonstrated below, (4.13) indicates that ξ_m is also approximately constant. Therefore, in terms of dimensional variables,

$$x_m b_0/d^2 \sim \theta_{crit}^{-1/(1-\gamma)} \left(\frac{C_6 \rho U_0^2 b_0^2}{\Delta \rho g d^3} \right)^{1/(1-\gamma)}. \tag{4.14}$$

This correlation is examined by plotting in figure 5(*b*) the experimentally determined

https://doi.org/10.1017/S0022112097005077 Published online by Cambridge University Press

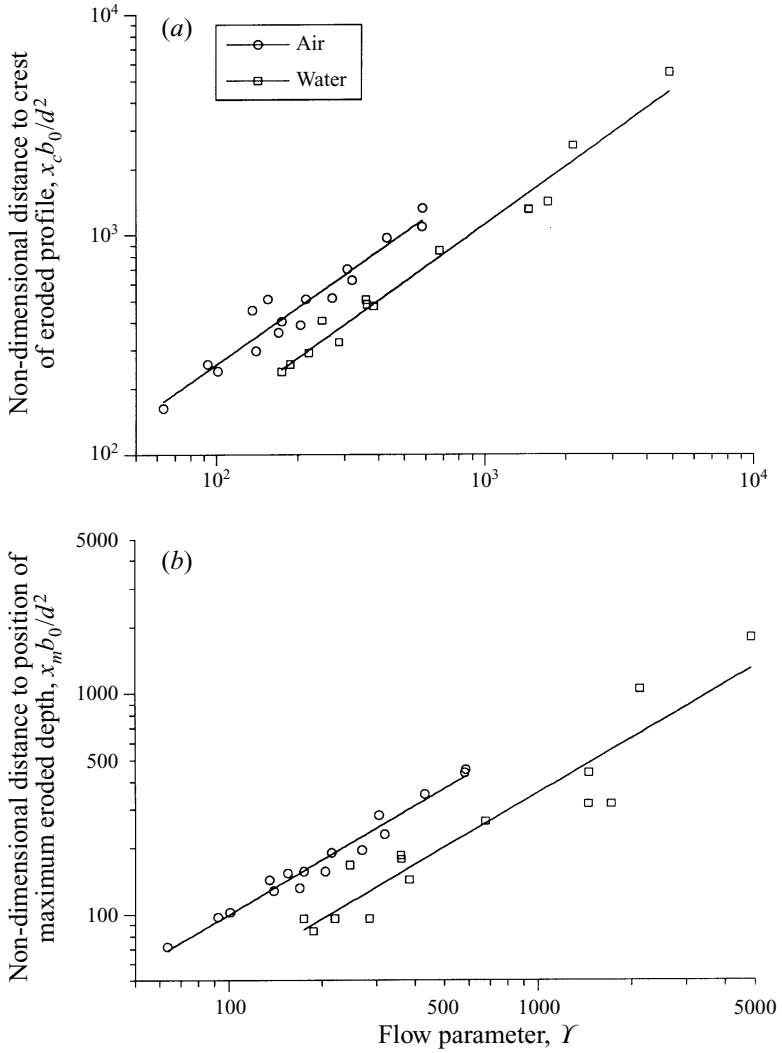


FIGURE 5. (*a*) The downstream distance to the peak of the eroded profile, x_c, as a function of the flow parameter, $\Upsilon = \rho U_0^2 b_0^2/\Delta\rho g d^3$. The equations of the fitted power-law curves are given by $x_c b_0/d^2 = 2.7\Upsilon^{0.87\pm0.04}$ (for water) and $x_c b_0/d^2 = 5.0\Upsilon^{0.85\pm0.06}$ (for air). (*b*) The downstream distance to the position of maximum eroded depth, x_m, as a function of the flow parameter $\Upsilon = \rho U_0^2 b_0^2/\Delta\rho g d^3$. The equations of the fitted power-law curves are given by $x_m b_0/d^2 = 1.3\Upsilon^{0.82\pm0.04}$ (for water) and $x_m b_0/d^2 = 2.3\Upsilon^{0.82\pm0.08}$ (for air). The confidence limits on the exponents are given by the standard errors of the best fitting values. (Data from Rajaratnam 1981.)

values of $x_m b_0/d^2$ against $\Upsilon \equiv \rho U_0^2 b_0^2/\Delta\rho g d^3$. There is a good correlation between these variables. Also, as for x_c, the data for the experiments performed with both air and water jets are collapsed by a power law, with a similar exponent. This exponent has the value $1/(1-\gamma) = 0.82$ which is similar to that determined for the variation of x_c. Furthermore, the different value of the constant for the two data series may be rationalized in terms of the magnitude of the critical Shields parameters for the two media.

In terms of the calculated solution (4.8)–(4.10), ξ_m and η_m vary as functions of the parameter σ, while ξ_c is independent of σ. From figure 6 ξ_m/η_m is approximately a

https://doi.org/10.1017/S0022112097005077 Published online by Cambridge University Press

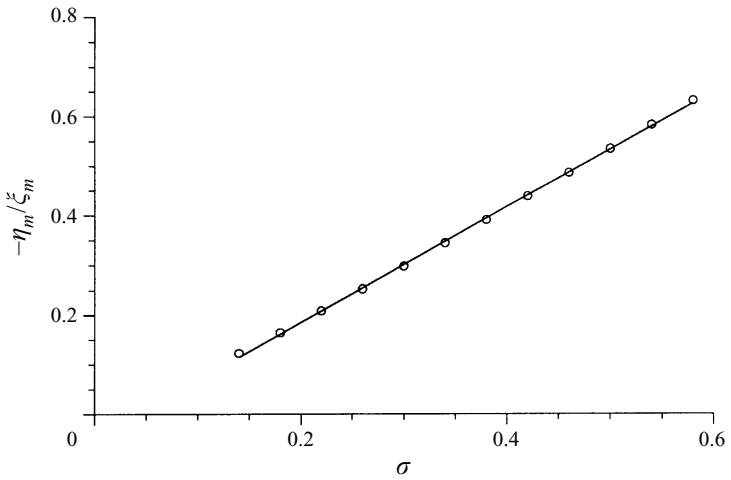


FIGURE 6. The ratio of the maximum eroded depth to the downstream location at which this occurs as a function of σ. The values of this ratio was computed from the model (§4) for a range of values of σ ($0.14 < \sigma < 0.58$). There is an approximately linear relationship between the two given by $\eta_m/\xi_m = 1.16\sigma - 0.05$.

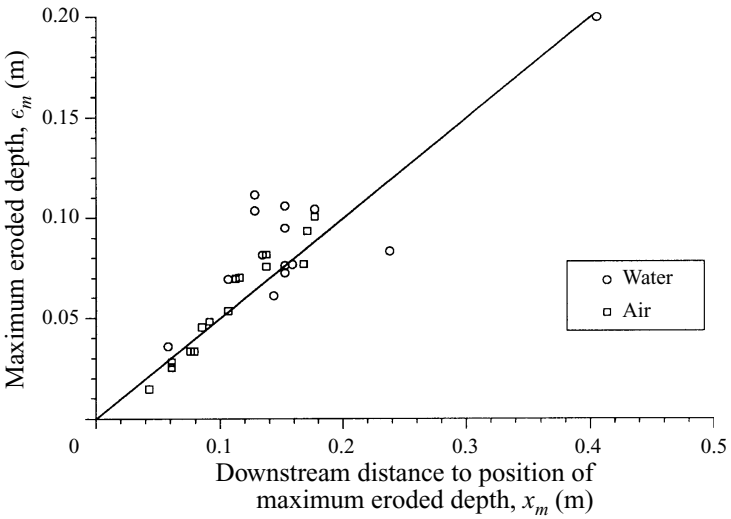


FIGURE 7. The maximum eroded depth ϵ_m as a function of the downstream distance to the position of maximum eroded depth x_m. The data for the experiments using both air and water wall jets are reasonably well represented by the linear equation $\epsilon_m = 0.5x_m$. (Data from Rajaratnam 1981.)

linear function of σ and $\eta_m \approx \sigma\xi_m$. Hence a plot of maximum scour depth ϵ_m against x_m for the experimental data should provide an estimate of the parameter σ. There is indeed a reasonable linear correlation between ϵ_m and x_m, with $\sigma = 0.5$ as indicated in figure 7. In accord with the theory developed here, this constant is the same for both sets of experiments.

The theoretically calculated profiles also elucidate the dependence of the ratio ξ_m/ξ_c on the parameter σ. We find that with increasing σ the position of maximum eroded depth moves closer to the source. This is because σ effectively represents the near-source spreading of the jet. Hence larger values of σ correspond to greater spreading

https://doi.org/10.1017/S0022112097005077 Published online by Cambridge University Press

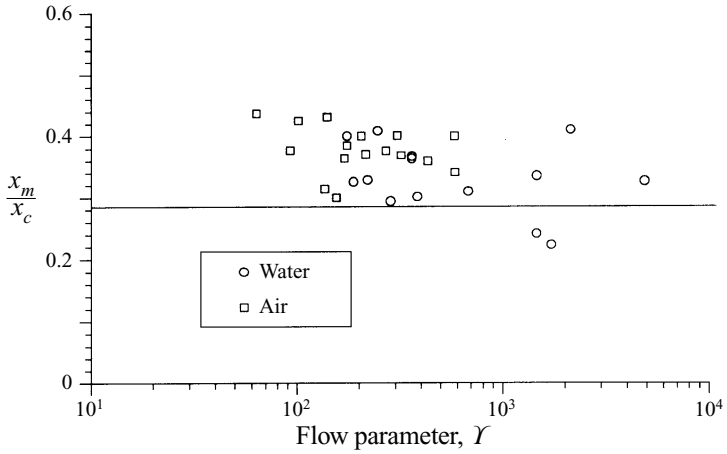


FIGURE 8. The ratio x_m/x_c as a function of the flow parameter Υ. The model predicts that $x_m/x_c = 0.28$, as drawn on the plot.

and therefore the maximum depth is attained closer to the source. The experimentally measured ratio of the dimensional distances ξ_m/ξ_c should be independent of the media in which the experiments were conducted and the theory predicts that $x_m/x_c = 0.28$ with $\sigma = 0.5$. This is approximately borne out in the experimental results of Rajaratnam (1981), as displayed in figure 8.

4.3. *Shape of eroded profile*

The profile of the scour pits may be calculated by the integration of (4.8) subject to the boundary conditions (4.9) and (4.10). The condition of a fixed volume of particles may not be entirely appropriate for comparison with experiments in which particles are swept downstream into a 'sand trap'. It is, however, appropriate for geophysical applications. In figure 9(*a*) we present the steady-state profiles for various values of the parameter σ. We note that for the profiles which correspond to larger values of σ, there are regions in which the upward inclination of the boundary exceeds the angle of repose. As argued in §3, these profiles may not be stable because the shear stress is intermittent. Hence they relax to a configuration in which the gradient of the upward slopes never exceeds the tangent of the angle of repose. We introduce this relaxation process via the following adjustment procedure, which is based upon the constancy of volume of the particles. Suppose that $\mathrm{d}\eta/\mathrm{d}\xi > \tan\alpha$, for some $\xi = \xi_0$ with $\xi^- < \xi_0 < \xi^+$. We then redefine the boundary profile as

$$\eta_{new}(\xi) = \begin{cases} \eta(\xi) & (\xi < \xi^-), \\ \eta(\xi^-) + (\xi - \xi^-)\tan\alpha & (\xi^- < \xi < \xi^+), \\ \eta(\xi) & (\xi > \xi^+). \end{cases} \tag{4.15a,b,c}$$

The limits ξ^- and ξ^+ satisfy the following two equations:

$$\eta(\xi^+) - \eta(\xi^-) = (\xi^+ - \xi^-)\tan\alpha \tag{4.16}$$

and

$$\int_{\xi^-}^{\xi^+} \eta \,\mathrm{d}\eta = \tfrac{1}{2}(\xi^+ - \xi^-)^2 \tan\alpha. \tag{4.17}$$

This adjustment for the profiles is shown in figure 9(*b*) and we note that it introduces negligible alteration to the overall shape of the scour pits.

https://doi.org/10.1017/S0022112097005077 Published online by Cambridge University Press

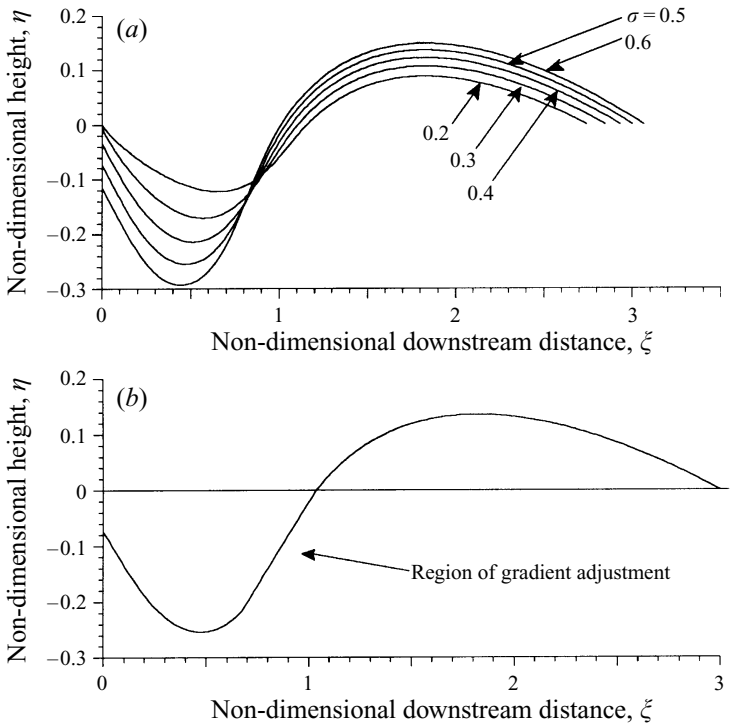


FIGURE 9. (*a*) The steady-state shape of the scour pit arising from the erosive action of a wall jet for various values of σ. (*b*) The steady-state shape of the scour pit arising from the erosive action of a wall jet, adjusted so that the maximum upward gradient never exceeds the tangent of the angle of repose for the particular value $\sigma = 0.5$. This adjustment introduces very little alteration of the shape of the profile.

Rajaratnam (1981) demonstrated the similarity of the steady-state shape of the eroded profiles by scaling the eroded depth by the maximum eroded depth ϵ_m and the distance from the source by the downstream distance to the position of maximum erosion x_m. He found that to a reasonable degree of accuracy this collapsed the profiles onto each other. We now compare the predicted eroded profiles with the experimentally measured profiles. We scale both the measured depth and the distance from the source by the distance to the maximum eroded depth (ξ_m). The agreement between theory and experiment is fairly good as seen in figure 10. This agreement is not too surprising, given that we have chosen the parameter $\sigma = 0.5$, although we have constrained neither the boundary condition at the source, nor the curvature of the profile (apart from imposing an upper bound on the gradient equal to the tangent of the angle of repose). The predicted and experimentally determined results differ around the downstream locations at which the profiles attain a maximal value. Presumably this difference arises because the model has neglected flow separation over the crest. Hence the model assigns a shear stress in excess of the true value and so predicts a downstream transport of particles which is too high. Instead, as the experimental results seem to show, there is increased particle deposition at the crest. Alternatively there may be a reverse flow at the lee side of the crest which could sweep particles towards the crest. A more complete model of the flow should rectify this discrepancy.

https://doi.org/10.1017/S0022112097005077 Published online by Cambridge University Press

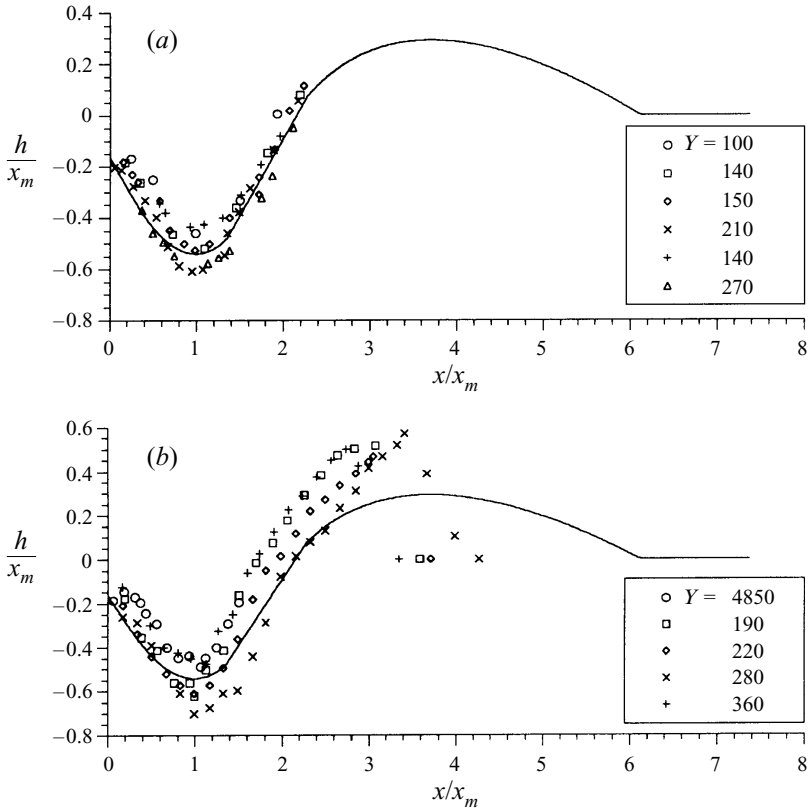


FIGURE 10. Comparison between the predicted and experimentally measured eroded profiles for the wall jets of (*a*) air and (*b*) water. (Data from Rajaratnam 1981).

5. Temporal evolution of the scour pit

While the theory developed above describes the shape of the steady-state eroded pits, it does not provide insight into their temporal evolution. Early studies of the rate of scour suggested that the maximum scour depth increases linearly with the logarithm of time (Rouse 1940) and is therefore unbounded. This suggestion has since been refuted as investigators have realized that a steady state is possible. Nevertheless the time taken to attain this steady state can be very long. For instance, Rajaratnam (1981) found that for some laboratory experiments, the attainment of the equilibrium profile of the scour pit took in excess of 60 hours. Furthermore, he found that at intermediate times the maximum eroded depth did approximately increase linearly with the logarithm of time.

In order to describe this temporal evolution we need to model the process of particle transport. The particles are non-cohesive and are primarily transported by rolling, sliding and saltating along the boundary, rather than by being launched into suspension and advected by the flow. We therefore adopt a bedload model of sediment transport (Nielsen 1992). This neglect of suspended-load sediment transport is probably a reasonable assumption for flows in which the density of the particles far exceeds that of the fluid; however for flows in which the two are comparable, it may considerably underestimate the rate of transport.

There are many empirical and semi-empirical models of bed-load transport (Fredsøe

https://doi.org/10.1017/S0022112097005077 Published online by Cambridge University Press

& Deigaard 1992), although in essence the dimensionless flux of particles depends upon the dimensionless shear stress raised to the 3/2 power. We adopt one of the oldest models, namely the semi-empirical model of Meyer-Peter & Muller (1948),

$$q_b/(\Delta\rho g d^3/\rho)^{1/2} = 8(\theta - \theta_c)^{3/2}, \tag{5.1}$$

where q_b is the dimensional volumetric flux of particles per unit width, $\theta = \tau_b/\Delta\rho g d$ is the Shields parameter and θ_c is the critical Shields parameter for incipient motion (see §3). The functional form of (5.1) was derived for particle transport on a flat bed, but we will apply it to a longitudinally sloping bed for which the critical Shields parameter varies with the local bed gradient. The recent study of Kovacs & Parker (1994) used a slightly different formula for the flux of bed-load transport to study the progressive erosion of a downstream step of bed elevation. We adopt the above expression because it takes a somewhat more simple functional relation. Many models of suspended sediment transport have a form similar to (5.1), except that the critical parameter for the onset of suspension is increased and the exponent of the Shields parameter is higher (Yalin 1977). Also models of cohesive soil transport take a similar form, but with a lower exponent (Stein *et al.* 1993).

Following Kovacs & Parker (1994), we study the temporal evolution of the pit by adopting a sediment conservation equation (the Exner equation). This relates the rate of change of the bed elevation to the divergence of the flux of particles. In two dimensions, this gives

$$(1 - C_b)\frac{\partial h}{\partial t} + \frac{\partial q_b}{\partial x} = 0, \tag{5.2}$$

where C_b is the porosity of the bed. We introduce non-dimensional variables for the lengthscales given by equations (4.4) and (4.5) and for the particle flux and timescale given by

$$\Psi = q_b/8(\theta_{crit}^3 \Delta\rho g d^3/\rho \tan^3\alpha)^{1/2} \tag{5.3}$$

and

$$T = t\frac{8(\theta_{crit}^3 \Delta\rho g d^3/\rho \tan^3\alpha)^{1/2}}{(1 - C_b)b_0^2 \Theta^{2/(1-\gamma)}}. \tag{5.4}$$

In non-dimensional form, the conservation equation is now given by

$$\frac{\partial \eta}{\partial T} + \frac{\partial \Psi}{\partial \xi} = 0. \tag{5.5}$$

We now substitute for the Shields parameter $\theta = f_b(\eta, \xi)\theta_{crit}/\tan\alpha$ and for the critical Shields parameter

$$\theta_c = \frac{\theta_{crit}}{\tan\alpha}\left(\frac{\partial\eta/\partial\xi + \tan\alpha}{\left(1 + (\partial\eta/\partial\xi)^2\right)^{1/2}}\right). \tag{5.6}$$

This yields the evolution equation

$$\frac{\partial \eta}{\partial T} = \tfrac{3}{2}(f_b - \theta_c \tan\alpha/\theta_{crit})^{1/2}\left(\frac{1 - \tan\alpha\,\partial\eta/\partial\xi}{(1 + (\partial\eta/\partial\xi)^2)^{3/2}}\right)\frac{\partial^2\eta}{\partial\xi^2} - \tfrac{3}{2}(f_b - \theta_c \tan\alpha/\theta_{crit})^{1/2}\frac{\partial f_b}{\partial\xi}. \tag{5.7}$$

This equation is subject to the following initial and boundary conditions:

$$\eta = 0 \qquad (T = 0), \tag{5.8}$$

$$\eta \to 0 \qquad (\xi \to \infty) \tag{5.9}$$

https://doi.org/10.1017/S0022112097005077 Published online by Cambridge University Press

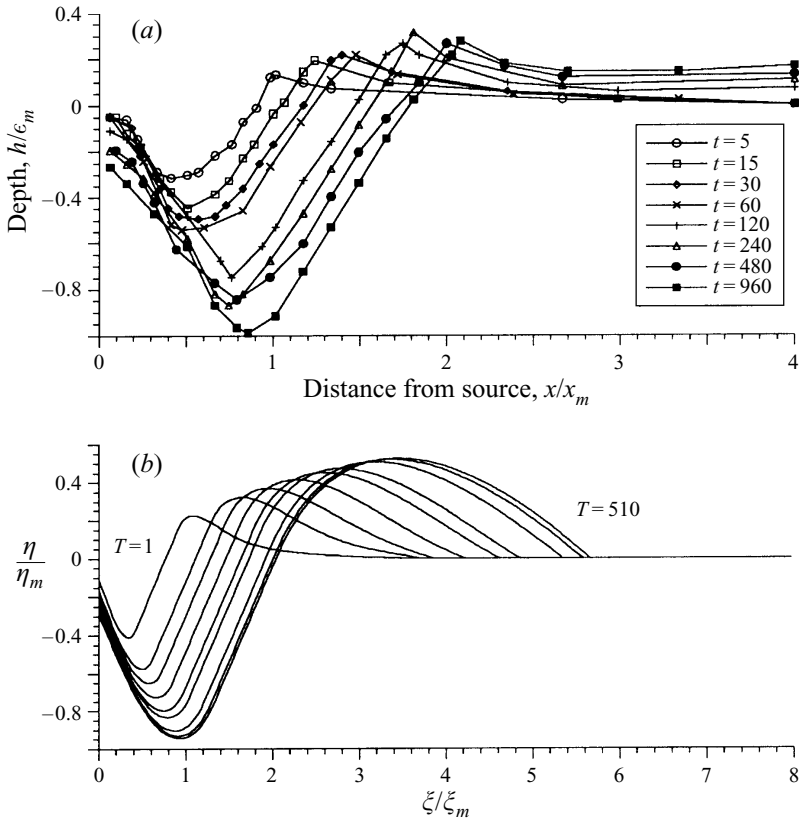


FIGURE 11. (*a*) Experimentally measured profiles (Rajaratnam 1981) at intermediate dimensional times (t) before the steady-state profile was attained. These profiles arose from the flow of an air wall jet over an initially flat bed of sand. The steady state was attained after approximately 15000 s. (*b*) Theoretically calculated profiles of an initially flat bed of grains at non-dimensional times of $T = 1, 5, 10, 20, 40, 60, 160, 310, 510$.

and

$$\theta - \theta_c = 0 \qquad (\xi = 0). \tag{5.10}$$

The interpretations of these equations are: the boundary is initially flat (5.8); there is no erosion sufficiently far downstream from the source of the jet (5.9); and there is no particle flux entering at the source of the jet flow (5.10). These boundary conditions imply that the volume of particles within the domain is constant, a condition which may be expressed as

$$\int_0^\infty \eta \, \mathrm{d}\xi = 0. \tag{5.11}$$

We note that equation (5.7) for the evolution of the bed elevation is effectively an advection–diffusion equation, with a nonlinear diffusion coefficient which depends upon ξ, η and $\partial\eta/\partial\xi$. When $\partial\eta/\partial\xi > \cot\alpha$, the effective diffusion coefficient becomes negative and the equation becomes ill-posed. The origin of this change of sign in the diffusion coefficient is that the magnitude of the critical Shields parameter for erosion on a sloping boundary has a maximum value at $\partial\eta/\partial\xi = \cot\alpha$.

We recall that the boundary shear stresses are intermittent (§3). Hence during the progressive erosion of an initially flat bed of particles, the applied shear stresses

https://doi.org/10.1017/S0022112097005077 Published online by Cambridge University Press

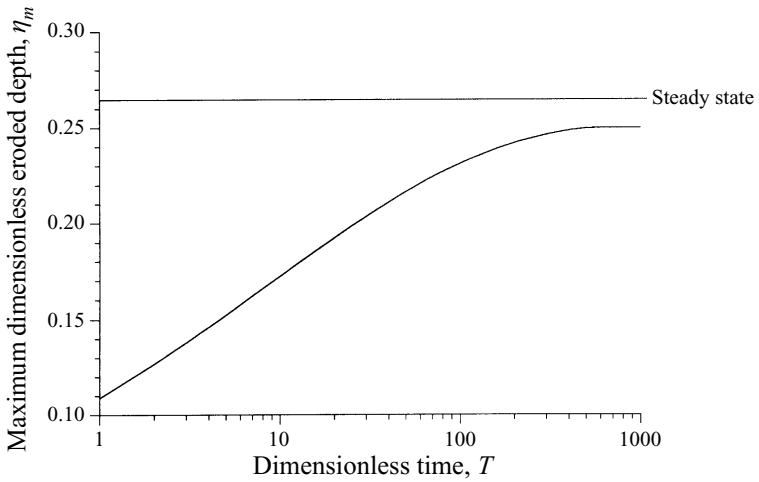


FIGURE 12. The maximum eroded depth as a function of non-dimensional time. Note that at intermediate times, before the steady state is attained, the maximum eroded depth varies linearly with the logarithm of time. (The steady-state eroded depth is $\eta_m = 0.265$.)

are insufficient to support upward gradients which exceed the tangent of the angle of repose. This hypothesis seems to be borne out by the observations made by Rajaratnam (1981) of the temporal development of the eroded profiles as shown in figure 11(*a*). Therefore we enforce a relaxation procedure after each timestep during the numerical integration of (5.7) to rearrange the profile such that $\partial\eta/\partial\xi < \tan\alpha$ for all ξ. We use a procedure identical to that described in §4.3 to enforce this bound on the maximum upward gradient.

We integrate (5.7) using a two-step numerical scheme which is analogous to the Crank–Nicholson scheme for differential equations with constant diffusivities (Press *et al.* 1986). When integrating between two timesteps ($\eta^n \rightarrow \eta^{n+1}$), we first take a half-timestep and use the values of $\eta^{n+1/2}$ to evaluate the diffusivity for the full timestep. After each full timestep we apply the rearrangement algorithm to ensure the upward gradients are less than $\tan\alpha$. This ensures the effective diffusion coefficient always remains positive and so the system remains well-posed. As a check on the numerical scheme, we evaluate $\int_0^\infty \eta\,\mathrm{d}\xi$ and ensure that

$$\int_0^\infty |\eta|\,\mathrm{d}\xi > \tfrac{1}{100}\left|\int_0^\infty \eta\,\mathrm{d}\xi\right|. \tag{5.12}$$

As an illustrative calculation we set $\gamma = 0$ and find the temporal development of the erosion profiles shown in figure 11(*b*). These profiles closely resemble those observed by Rajaratnam (1981). We plot the temporal development of the maximum scour depth in figure 12. We find that for intermediate times there is indeed a period when the maximum scour depth increases approximately linearly with the logarithm of time. We note that the implementation of an upper bound on the gradient of the profile after each timestep may influence the steady state attained by (5.7)–(5.10) because during each timestep the number of particles moved downstream may be exactly balanced by those moved upstream by the relaxation procedure. In calculating the results of the integration of the equations, shown in figures 11(*b*) and 12, the timestep was equal to one non-dimensional unit at large times and we find that we achieve a steady-state maximum eroded depth within 2% of that calculated in §4. For

https://doi.org/10.1017/S0022112097005077 Published online by Cambridge University Press

a subsequent run in which the timestep at large times was 10 non-dimensional units the steady-state maximum eroded depth was to within 0.5% of that calculated in §4.

The timescale of the erosion may be estimated from the temporal scaling given by equation (5.4). For the specific conditions of the experiment performed by Rajaratnam (1981), for which the temporal development of the eroded profiles is plotted in figure 11(*a*), we find that a dimensionless unit of time corresponds to approximately 10 s. The numerical integration of the Exner equation (5.7) demonstrates that it is not until the jet has been flowing for 100 dimensionless units of time that the maximum eroded depth attains approximately 90% of its steady-state value. Hence for the specific experimental conditions, which correspond to the profiles plotted in figure 11(*a*), this is equivalent to a duration of 1000 s. This estimate is consistent with the experimental observations which indicated a relatively rapid rate of erosion during the first 1000 s of the jet flow, followed by a much slower rate of erosion until the steady state was attained after approximately 15000 s (Rajaratnam 1981).

6. Conclusion

We have considered the erosive action of a two-dimensional turbulent wall jet on an initially flat bed of non-cohesive particles and have elucidated a number of features of this process. We have demonstrated that turbulent wall jets, flowing over rough boundaries, may not be simply approximated by the free-jet scalings, because these neglect the importance of the boundary. Instead the spatial variation of the wall-jet characteristics are weakly dependent on the roughness length of the boundary (§2).

We have modified the results for flows over fixed boundaries to study those over erodible boundaries. We balanced the mobilizing and resisting moments on the particles at the surface of the sloping bed, to obtain critical conditions for incipient particle motion. This enables the prediction of the characteristic dimensions of the steady-state scour pit to be made and reconciles the previously unresolved differences between the experiments performed with air and water jets. By adopting a simple model of the distribution of shear stress, the shape of the eroded profiles was found to be in good agreement with the experimental results. The calculation of steady-state erosion profiles relied on a simple model of the distribution of shear stress, which neglects regions of flow separation and recirculation. While future developments will no doubt contribute to an improved model of the flow, the simple approach described here has enabled the explanation of many of the experimental results of Rajaratnam (1981).

We have also formulated a model of the progressive erosion of the scour pit. This model invokes a bed-load model of the rate of particle transport and follows the evolution of the bed by utilizing an expression for the conservation of sediment volume. Inherent in such an approach are a number of additional assumptions. This model neglects, for example, the particles which are transported downstream in suspension. Nevertheless, this analysis produces eroded profiles which are similar to those found experimentally. We find that the maximum eroded depth at intermediate times varies linearly with the logarithm of time, and that the time taken to achieve the steady-state erosion can be very long. This has significant implications for the operation of jet-scour devices, because there is a trade-off between the volume of mobilized sediment and the time during which the jet impinges upon a particular area of the bed. Ongoing research will aid the development of optimum operational procedures.

The financial support of the Ministry of Agriculture, Fisheries and Food (UK) and NERC is gratefully acknowledged.

https://doi.org/10.1017/S0022112097005077 Published online by Cambridge University Press

Appendix. Incipient motion on a sloping bed

In this Appendix we derive the critical conditions for incipient particle motion for a spherical particle in repose on a planar bed, composed of similar particles, which has both longitudinal and lateral slopes. This calculation yields a critical Shields parameter which is in accord with previous expressions (Fredsøe & Deigaard 1992). Kovacs & Parker (1994) developed a vectorial formulation of this problem and obtained expressions for the critical Shields parameter. The analysis developed below is also a vectorial formulation of the critical conditions for particle motion but is based upon the turning moments exerted on a particle at the bed surface and the angle of repose, rather than the mobilizing forces and a friction coefficient used by Kovacs & Parker (1994). Nevertheless, it yields results which are identical to those of Kovacs & Parker. In this analysis we identify the angle of repose as the maximum inclination of the free surface of a given granular material at which there is no particle motion, in the absence of any other flow (Savage 1989).

We consider a particle in repose on a planar, but non-horizontal bed, over which fluid flows. The fluid motion exerts a torque on the particle which is resisted by the stabilizing moment arising from the particle weight. We define an orthonormal basis of vectors for this plane $(\hat{\boldsymbol{n}}, \hat{\boldsymbol{s}}, \hat{\boldsymbol{t}})$, where $\hat{\boldsymbol{n}}$ is the normal to the plane, $\hat{\boldsymbol{s}}$ is parallel with the direction of flow and $\hat{\boldsymbol{t}} = \hat{\boldsymbol{n}} \times \hat{\boldsymbol{s}}$. The angle between the flow direction and the direction of steepest descent on the plane is denoted by ψ and the angle of inclination of the plane is β. Hence a vertical unit vector is given by

$$\hat{\boldsymbol{y}} = \cos\beta\hat{\boldsymbol{n}} + \sin\beta(\cos\psi\hat{\boldsymbol{s}} - \sin\psi\hat{\boldsymbol{t}}). \tag{A 1}$$

At incipient motion, a particle pivots on the adjacent particles at the angle of repose with a direction which makes an angle ϕ with the direction of flow. Hence a unit vector between the axis of rotation and the centre of the particle is given by

$$\hat{\boldsymbol{r}} = -\cos\alpha\hat{\boldsymbol{n}} + \sin\alpha(\cos\phi\hat{\boldsymbol{s}} + \sin\phi\hat{\boldsymbol{t}}). \tag{A 2}$$

The flow exerts a drag force on the particle given by

$$\boldsymbol{F} = C_D\pi d^2\tau_b\hat{\boldsymbol{s}}, \tag{A 3}$$

where τ_b is the shear stress, d is the particle diameter and C_D is a constant drag coefficient. The submerged particle weight is

$$\boldsymbol{W} = -\tfrac{1}{6}\pi\Delta\rho g d^3\hat{\boldsymbol{y}}, \tag{A 4}$$

where $\Delta\rho$ is the excess density and g is the gravitational acceleration. Denoting the moment of inertia and angular velocity of the particle by I and $\boldsymbol{\Omega}$, respectively, we find that the equation of motion of the particle is given by

$$I\frac{\mathrm{d}\boldsymbol{\Omega}}{\mathrm{d}t} = (\boldsymbol{W} + \boldsymbol{F}) \times d/2\hat{\boldsymbol{r}}. \tag{A 5}$$

Hence the particle is set into motion if $(\boldsymbol{W} + \boldsymbol{F}) \times d/2\hat{\boldsymbol{r}} > 0$. This condition yields the following expression:

$$\begin{aligned}\frac{6C_D\tau_b}{\Delta\rho g d}\left(\cos\alpha\hat{\boldsymbol{t}} + \sin\alpha\sin\phi\hat{\boldsymbol{n}}\right) > {} & (\cos\alpha\sin\beta\cos\psi + \cos\beta\sin\alpha\cos\phi)\,\hat{\boldsymbol{t}} \\ & + (\cos\alpha\sin\beta\sin\psi - \cos\beta\sin\alpha\sin\phi)\,\hat{\boldsymbol{s}} \\ & + (\sin\psi\sin\beta\sin\alpha\cos\phi + \cos\psi\sin\beta\sin\alpha\sin\phi)\,\hat{\boldsymbol{n}}.\end{aligned} \tag{A 6}$$

https://doi.org/10.1017/S0022112097005077 Published online by Cambridge University Press

At incipient motion, we identify the critical value of the Shields parameter $\theta_c = \tau_b/\Delta\rho g d$ and find that

$$|\sin\phi| = \left|\frac{\tan\beta\sin\psi}{\tan\alpha}\right| < 1, \tag{A 7}$$

$$6C_D\theta_c = \sin\beta\cos\psi + \sin\psi\sin\beta\cot\phi. \tag{A 8}$$

The condition (A7) specifies the direction of motion and gives a criterium which if exceeded implies that the bed is unstable and 'slumping' occurs. The condition (A8) may be rewritten in terms of the angles of repose, longitudinal and lateral slopes (α, β, ψ) and the critical Shields parameter on a flat bed, $\theta_{crit} = \frac{1}{6}\tan\alpha/C_D$, as

$$\theta_c = \theta_{crit}\left(\frac{\cos\psi\sin\beta + (\cos^2\beta\tan^2\alpha - \sin^2\psi\sin^2\beta)^{1/2}}{\tan\alpha}\right). \tag{A 9}$$

REFERENCES

Fredsøe, J. & Deigaard, R. 1992 *Mechanics of Coastal Sediment Transport*. World Scientific.

Glauert, M. B. 1956 The wall jet. *J. Fluid Mech.* **1**, 625–643.

Greeley, R. & Iversen, J. D. 1985 *Wind as a Geological Process*. Cambridge University Press.

Kline, S. J., Reynolds, W. C., Schraub, F. A. & Runstadler, P. W. 1967 The structure of turbulent boundary layers. *J. Fluid Mech.* **30**, 741–773.

Kobus, H., Leister, P. & Westrich, B. 1979 Flow field and scouring effects of steady and pulsating jets impinging on a movable bed. *J. Hydr. Res.* **17**, 175–192.

Kovacs, A. & Parker, G. 1994 A new vectorial bedload formulation and its application to the time evolution of straight river channels. *J. Fluid Mech.* **267**, 153–183.

Launder, B. E. & Rodi, W. 1983 The turbulent wall jet-measurements and modelling. *Ann. Rev. Fluid Mech.* **15**, 429–459.

Luque, R. F. 1974 Erosion and transport of bed-load sediment. PhD Thesis, Delft Hydraulics Institute.

Mason, P. J. & Arumugam, K. 1985 Free jet scour below dams and flip buckets. *J. Hydr. Engng.* **111**, 220–235.

Meyer-Peter, E. & Muller, R. 1948 Formula for bed-load transport. *Proc. Intl Assoc. Hydr. Struct. Res. Stockholm*, pp. 39–64.

Mih, W. C. & Kabir, J. 1981 Impingement of water jets on non-uniform streambed. *J. Hydr. Engng.* **109**, 536–548.

Nielsen, P. 1992 *Coastal Bottom Boundary Layers and Sediment Transport*. World Scientific.

Press, W. H., Teukolsky, S. A., Vetterling, W. T. & Flannery, B. P. 1986 *Numerical Recipes*. Cambridge University Press.

Rajaratnam, N. 1967 Plane turbulent wall jets on rough boundaries. *Water Power* **19**, April, May, June

Rajaratnam, N. 1976 *Developments in Water Sciences: Turbulent jets*. Elsevier.

Rajaratnam, N. 1981 Erosion by plane turbulent jets. *J. Hydr. Res.* **19**, 339–358.

Rajaratnam, N. 1982 Erosion by submerged circular jets. *J. Hydr. Div. ASCE* **108**, 262–266.

Rajaratnam, N., Aberibigbe, O. & Pochylko, D. 1995 Erosion of sand beds by oblique plane water jets. *Proc. Inst. Civ. Engrs Wat. Marit. Energy* **112**, 31–38.

Rajaratnam, N. & Beltaos, S. 1977 Erosion by impinging circular turbulent jets. *J. Hydr. Div. ASCE* **103**, 1191–1205.

Rajaratnam, N. & Berry, B. 1977 Erosion by circular turbulent wall jets. *J. Hydr. Res.* **15**, 277–289.

Rouse, H. 1940 Criteria for similarity in the transportation of sediment. *Proc. 1st Hydr. Conf., State University of Iowa, Iowa*, pp. 43–49.

Savage, S. B. 1989 Flow of granular materials. In *Theoretical and Applied Mechanics* (ed. P. Germain, M. Piau, D. Caillerie), pp. 241–266. IUTAM.

Shields, I. A. 1936 Anwendung der Aehnlichkeitsmechanik und der Turbulenz-forschung auf die Geschiebewegung. *Mitt. Preuss. Versuchsanstalt Berlin 26.*

https://doi.org/10.1017/S0022112097005077 Published online by Cambridge University Press

Stein, O. R., Julien, P. Y. & Alonso, C. V. 1993 Mechanics of jet scour downstream of a headcut. *J. Hydr. Res.* **31**, 723–738.

Wiegel, F. W. 1980 *Fluid Flow through Porous Macromolecular Systems*. Lecture Notes in Physics, vol. 121. Springer.

Wygnanski, I., Katz, Y. & Horev, E. 1992 On the applicability of various scaling laws to the turbulent wall jet. *J. Fluid Mech.* **234**, 669–690.

Yalin, M. S. 1977 *Mechanics of Sediment Transport*. Pergamon Press.

https://doi.org/10.1017/S0022112097005077 Published online by Cambridge University Press